Interfacial and structural relaxations of snow under isothermal conditions

H. LÖWE, J.K. SPIEGEL, M. SCHNEEBELI

WSL Institute for Snow and Avalanche Research SLF, Flüelastrasse 11, CH-7260 Davos-Dorf, Switzerland
E-mail: loewe@slf.ch

ABSTRACT. We investigated the morphological evolution of laboratory snow under isothermal conditions at $-3, -9$ and $-19°C$, using X-ray tomography. We employed a two-point density correlation function to measure spatial fluctuations of the density of the bicontinuous ice/vapor system at different length scales. Length scales were derived from the correlation function to distinguish between interfacial coarsening due to the minimization of surface energy on the smallest scales and anisotropic structural re-arrangements due to gravity on larger scales. On the smallest scales our data suggest a crossover between $T = -9$ and $-19°C$ from evaporation/condensation to surface diffusion as the dominant transport mechanism. Anomalous growth was found for the slope of the correlation function at the origin, and it was similar to those reported for the coarsening of fractal clusters. This is consistent with the observed persistence of dendritic structures throughout an entire year. The dynamics of large-scale morphology was characterized by the first zero-crossing of the correlation function which displays a nonmonotonic evolution with a pronounced anisotropy between the direction of gravity and horizontal directions. Since the correlation function naturally emerges in problems of scattering of radiation in snow, our results appear to be important for optical and remote-sensing methods.

INTRODUCTION

Snow crystals exhibit a variety of morphological changes which are driven by fundamentally different thermodynamic conditions. During growth in the atmosphere the problem can be well described by an isolated crystal in a supersaturated environment, which is a classical problem of single-crystal growth (Saito, 1996). If the orientation of the crystal is taken into account, growth velocities can be measured on the singular surfaces (Libbrecht, 2003) and the snow morphology or Nakaya diagram (Furukawa and Wettlaufer, 2007) can be reasonably well explained in terms of temperature, supersaturation and crystal properties (see Libbrecht, 2005, for a review). If these non-equilibrium growth forms are deposited on the ground to form a seasonal snowpack the crystals no longer evolve in isolation. Structural correlations may be built up during atmospheric aggregation (Westbrook and others, 2004) or during deposition on the ground (Löwe and others, 2007). The subsequent evolution of the deposit is dominated by collective behavior of the crystal packing on different length scales. A unique characteristic of this packing is its bicontinuous nature, where both phases (ice and vapor) occupy a singly connected region in space. Gravity does not permit isolated ice crystals or isolated pores, i.e. vapor bubbles do not emerge until bubble close-off at volume fractions of ~0.9 (Arnaud and others, 2000). The simplest cases of thermodynamic conditions are isothermal conditions where the relaxation to equilibrium is commonly referred to as isothermal metamorphism.

Previous work on isothermal metamorphism focused on possible transport mechanisms for the origin of interfacial relaxation (see Blackford, 2007, for a review). It is widely believed that evaporation/condensation of vapor is the dominant process of mass transport (Dominé and others, 2003; Legagneux and others, 2004; Legagneux and Dominé, 2005). The dynamical evolution of ice morphology is then usually characterized in terms of specific surface area, which is the interfacial area of the ice/vapor interface per ice volume (Dominé and others, 2003; Flin and others, 2003; Legagneux and others, 2004; Kaempfer and Schneebeli, 2007). Sometimes an ice thickness is used (Kaempfer and Schneebeli, 2007), which is derived from a pore-size distribution of the ice phase. Another quantity monitored during isothermal metamorphism is the mean curvature (Flin and others, 2003, 2004). The evolution of the aforementioned quantities is then related to grain growth (Legagneux and others, 2004), sintering theory (Kaempfer and Schneebeli, 2007) or a mean-field approach (Legagneux and Dominé, 2005), which is closely related to the Lifshitz–Slyozov–Wagner (LSW) theory of Ostwald ripening (Lifshitz and Slyozov, 1961; Wagner, 1961).

The majority of concepts put forward for isothermal metamorphism have two main shortcomings. First, LSW-type approaches usually employ a geometry which consists of spheres and neglects the bicontinuous nature of the ice matrix in snow. This makes it difficult to relate deviations of experiments from theory, either to deficiencies of the ice-phase geometry or to deficiencies of the physics which underlies LSW. Second, neither of the quantities employed to characterize the dynamics can detect anisotropic behavior. In view of the fact that gravity breaks the symmetry between vertical and horizontal directions, there is a demand for an orientation-dependent characterization which addresses the interplay between gravitational and surface energy. Though the recent Monte Carlo approach (Vetter and others, 2010) does not have geometrical limitations, its comparison with experiments is still based on nondirectional quantities, such as the surface area or the ice thickness. There is a need to develop more distinguishing measures of isothermal metamorphism to provide a benchmark for theoretical models.

To contribute in this direction, we address isothermal metamorphism from a different perspective. The focus of the present paper is an anisotropic, multiple-scale characterization of isothermal metamorphism by means of spatial fluctuations of the microscopic density, or phase field,
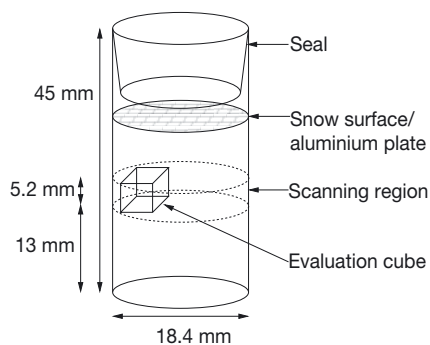
45 mm — Seal

Snow surface/
aluminium plate

5.2 mm — Scanning region

13 mm — Evaluation cube

18.4 mm

Fig. 1. Schematic of the cylindrical tomography sample holder.

$\phi(\mathbf{x}, t)$, as a function of position, $\mathbf{x}$, and time, t. We employ X-ray tomography to measure $\phi(\mathbf{x}, t)$ with high spatial resolution throughout an entire year for different temperatures, and take the novel approach of characterizing the dynamics by the anisotropic two-point correlation function. To strictly control the initial conditions, we use laboratory snow with crystals grown from vapor which are subsequently deposited into sample holders by sieving. By comparing the evolution of various length scales we are able to identify relevant scales and their interaction from different relaxation mechanisms during metamorphism.

This paper is organized as follows: The experimental set-up is described in the next section. In the following section we describe our conceptual starting point. Subsequently we provide definitions of the correlation function and a thickness distribution and define various length scales. The measurement results for all quantities are then presented, followed by conclusions and suggestions for future work in the final section.

EXPERIMENTS

Our general experimental set-up for the X-ray tomography follows Kaempfer and Schneebeli (2007), with two important differences for the sample handling: (1) the isothermal storage was further improved to minimize the effect of predominant temperature gradients and (2) laboratory-generated new snow was used to guarantee similar initial conditions for the snow samples at different temperatures. Details are given below.

Snow sample preparation

All snow samples were prepared from laboratory snow which was produced in a simple snowmaker, with a design that basically follows Nakamura (1978). A heated water reservoir is kept at a temperature of $T = 30°C$ in a cold room environment at $T = -25°C$. The humid air above the water surface is continuously advected by a fan into a box at ambient temperature, where the vapor precipitates on thin nylon wires which serve as growth nuclei. By varying air and water temperature the method is able to qualitatively reproduce growth modes and crystal habits predicted by the Nakaya diagram (Furukawa and Wettlaufer, 2007). The ambient temperature in the vicinity of the wires was $T \approx -18°C$ and under these conditions growth is mainly dendritic. Snow crystals are periodically harvested from the wires by automatic vibration. The manufactured snow powder compact had a density $\rho \approx 172\,kg\,m^{-3}$. With an ice density $\rho_{ice} = 917\,kg\,m^{-3}$ this amounts to an

initial volume fraction $\phi_i = 0.188$. The snow was stored for 24 hours at $-25°C$ to allow for moderate, initial sintering of the crystals. Using a sieve with a mesh size of 2 mm, the snow was sieved into cylindrical sample holders (Fig. 1) until they were completely filled. The snow was then slowly compressed to provide space for the seal and avoid local densification of the top part when the seal was inserted. Before sealing, a small (0.2 g) aluminium weight was placed on top of the sieved snow to provide a reference line for the snow surface in the sample holder. There was always a gap between the aluminium plate and the seal, which increased throughout the experiment due to densification. For the seal we used a low-density polyethylene cap to avoid sublimation and obtain a closed system with respect to mass exchange.

Sample storage

Overall, three identical snow samples under three different isothermal conditions (-3, -9 and $-19°C$) were examined using microcomputed-tomography scanning over the course of 1 year. To improve the isothermal conditions, the storage boxes used by Kaempfer and Schneebeli (2007) were adapted to reduce thermal gradients. The storage boxes are constructed using layers of highly insulating and highly conducting materials. The highly conducting material with high heat capacity (steel) prevents the build-up of a temperature inversion in the air, and eliminates temperature fluctuations. From the inside out, the packaging was constructed as follows: The sample cylinders were fixed in a Styrofoam^{TM} mask inside a steel cylinder with 1 cm thick walls. The steel cylinders were capped from both sides with 1 cm thick steel lids. This steel cover was packed into a small Styrofoam box with 5 cm thick walls. The box was again surrounded by 5 mm thick steel plates and then enclosed in a vacuum-insulated box. The improvement over the previous storage box was an additional conducting layer and the vacuum-insulated box in the packaging. The temperature was recorded inside each steel cylinder by two temperature sensors (iButtons DS1922L). These sensors have an accuracy of $\pm 0.5°C$ (from -10 to $+65°C$) and a resolution of $0.0625°C$. They were calibrated before the measurements. Recorded temperatures were almost constant, with mean values and standard deviations of $T = -3.7 \pm 0.7°C$ (sample 1), $T = -9.5 \pm 0.1°C$ (sample 2) and $T = -18.6 \pm 0.8°C$ (sample 3). This corresponds to homologous temperatures of 0.99, 0.97 and 0.93.

Tomography

At the beginning of the experiment each sample is measured at ~ 3 week intervals. Since the evolution slows down during the experiment (Kaempfer and Schneebeli, 2007) we decreased the measuring frequency in the late stage of the experiment. For measurements the samples were transported from the storage room in a small Styrofoam box. The computed-tomography (CT) scanning (micro-CT 80, Scanco) was done with a nominal resolution (pixel size) of 10 μm and a modulation transfer function at 10% contrast level of 12.4 μm. The scanning region was fixed in space at 13 mm height from the bottom of the sample holder (Fig. 1). The height of the scanning region was 5.2 mm (520 voxels). The CT chamber was kept close to the nominal storage temperatures (-3, -9 and $-19°C$). After measurement the sample was placed in the transport box and returned to the storage box.

From the attenuation image of the scanned region a cube of 520^3 voxels = 5.2 mm^3 was extracted (Fig. 1), which was twice as large as the representative volume of 1–2 mm for the considered properties (Kaempfer and others, 2005). The grayscale images were filtered using a Gaussian filter with a kernel size of 5^3 and standard deviation of 1.2 voxels to improve the signal-to-noise ratio. A binary image was then obtained by segmentation of the filtered data. A single segmentation threshold was used for all images. This threshold was the average over thresholds determined for each sample individually such that its density was matched.

THEORETICAL BACKGROUND
Phase-ordering dynamics

Isothermal metamorphism of snow can be conveniently described (Legagneux and Dominé, 2005) by coarsening following the basic principles of the LSW theory of Ostwald ripening (Lifshitz and Slyozov, 1961; Wagner, 1961). The LSW idea can be summarized as mass transport between spheres of different radii, driven by chemical potential differences due to the Gibbs–Thompson condition. (For details and variants of LSW see Ratke and Voorhees, 2002.) The LSW theory assumes an assembly of spheres which imposes a severe limitation on admissible microstructural geometries. As a consequence, apparent deviations of experiments from theory cannot be unambiguously traced back either to deficiencies of the ice-phase geometry or to deficiencies of the physics which underlie LSW. It is therefore desirable to discuss isothermal metamorphism of snow in a wider context, where the geometrical constraints can be relaxed.

It has long been recognized that Ostwald ripening is a particular example of coarsening which can be found in many systems undergoing phase ordering or phase separation (see Bray, 1994, and references therein). In this context the dynamics of phase morphologies is studied via evolution equations for a so-called 'order parameter field' which describes the spatio-temporal distribution of the phases. For dry snow the phases are solid ice and vapor and a suitable order parameter is a phase-field function, ϕ, attaining $\phi = 1$ in the ice phase and $\phi = -1$ in the vapor phase (Kaempfer and Plapp, 2009). The most prominent phase-field models are the Cahn–Hilliard or Allen–Cahn equations, which describe the dynamics of a conserved or nonconserved order parameter, respectively (Balluffi and others, 2005). The terminology discriminates whether or not phase changes, as described by an order parameter, are locally constrained by a conservation law. Though these models provide a highly idealized starting point, they essentially contain the same physics as LSW (Wang, 2008) and can be applied to arbitrary microstructures. Thus results obtained for these phase-field models are also of relevance for isothermal metamorphism.

In general, the dynamics of microstructures is characterized by evolving length scales. This is often employed via a growth form, $R(t)^z - R(0)^z = Kt$ (Gow, 1969; Legagneux and others, 2004) for the mean radius, $R(t)$, in terms of the growth rate, K, and an exponent, z (which we refer to as the 'dynamic exponent' hereafter). This form is a characteristic of the LSW analysis, and there is no a priori justification for a generalization to $l(t)^z - l(0)^z = K't$ for different length scales, l, with a different rate, K', in arbitrary microstructures. We note, though, that this generalization works reasonably well

for the ice thickness in the work of Kaempfer and Schneebeli (2007). Henceforth, however, we restrict ourselves to the power-law form, $I \sim t^{1/z}$, which can be likewise inferred for long times from the LSW growth law given as $R(t) \sim t^{1/z}$.

It is widely accepted (Bray, 1994) that the value of the dynamic exponent, z, is essentially dependent on whether the order parameter is conserved or nonconserved. In either case, all length scales, l, will evolve with the same power law, $l \sim t^{1/z}$, for long times, where $z = 3$ for Cahn–Hilliard (conserved) and $z = 2$ for Allen–Cahn (nonconserved) dynamics. These two cases correspond precisely to the two cases addressed in LSW theory, namely transport limited by surface kinetics and diffusion in the gas phase. Both cases are treated by Lifshitz and Slyozov (1961), whereas Wagner (1961) considers only the kinetics-limited case. A crossover between these cases can be achieved by a variation of either the diffusion constant of vapor or the kinetic coefficient (Libbrecht, 2005) which controls the attachment kinetics of vapor molecules on the ice surface. The observed crossover between $z = 2$ and $z = 3$ in the mean-field model (Legagneux and Dominé, 2005) triggered by a variation of the kinetic coefficient is thus a direct implication of the underlying universality classes of conserved or nonconserved dynamics.

It is interesting that both exponents have also been verified in simulations of the Cahn–Hilliard or Allen–Cahn equations for coarsening of bicontinuous structures (Kwon and others, 2007). In both cases the so called 'dynamic scaling' hypothesis has been verified. This means that in either case the system is truly characterized by a single length scale, $l \sim t^{1/z}$. Given the connection of Cahn–Hilliard or Allen–Cahn dynamics to snow metamorphism, three main implications can be drawn from Kwon and others (2007): (1) the bicontinuous nature of the ice matrix has no a priori influence on the exponents (they are not a distinctive feature of the approximation of the geometry by spheres used in LSW theory); (2) the evolution of snow should be governed by $z = 2$ or $z = 3$ if no additional mechanisms play a role besides those contained in LSW; (3) any of the commonly investigated quantities, such as specific surface area, mean or Gaussian curvature or ice thickness, can be used in the same way as the characteristic length scale. All should evolve with the same power-law exponent, z.

Indeed we expect that snow displays deviations from this idealized dynamics. This is a consequence of emerging, competing length scales. The origin of additional scales can roughly be distinguished by the following cases: (1) transient behavior from initial conditions which may involve a wide distribution of persistent length scales and (2) the emergence of additional physical mechanisms beyond LSW. Signatures of different competing length scales can easily be detected by the behavior of length distribution functions. If these distributions are rescaled by their time-dependent mean but fall onto a single master curve (data collapse), different length scales must evolve under different dynamics. This has been observed by Legagneux and Dominé (2005) for the curvature distribution in snow. This breakdown of dynamic scaling may, however, be due to either case 1 or 2 mentioned above.

It is thus inevitable that a scale-dependent characterization of the microstructure must be used, which can be objectively defined for bicontinuous media. Though interfacial curvature distributions are popular (Mendoza and others, 2005) and have been applied to snow (Legagneux and Dominé, 2005), the interpretation of the observed absence of data collapse and the inclusion of anisotropic behavior is rather difficult.

We therefore follow the traditional route of characterizing heterogeneous systems and investigate the equal-time, two-point correlation function of the microscopic density which has been widely used to characterize random media (Torquato, 2002). The long tradition of using the correlation function for disordered systems stems from the fact that its Fourier transform is directly accessible via the scattering intensity obtained from small-angle scattering (Debye and Bueche, 1949). This relation to scattering intensity is also the foundation of the applicability of the correlation function to optical properties of snow (Vallese and Kong, 1981; Mätzler, 1998; Wang and others, 1998). For snow optics, the correlation function is required to interpret scattering from remote-sensing or field measurements. The correlation function has also been used for stochastic reconstruction of snow microstructure to study mechanical properties of high-density snow (Yuan and others, 2010).

Two-point correlation function

For time-dependent, continuous mass distributions the microscopic density is defined in terms of the phase indicator function, $\phi_i(\mathbf{x}, t)$, of the ice phase, which is defined by $\phi_i(\mathbf{x}, t) = 1$, if at time t the three-dimensional position vector, $\mathbf{x}$, lies in the ice phase and zero otherwise. The microscopic mass density, $\rho_i(\mathbf{x}, t)$, is related to ϕ_i by the intrinsic density of ice ($\rho_{ice} = 917 \, \mathrm{kg \, m^{-3}}$) via

$$\rho_i(\mathbf{x}, t) = \rho_{ice} \, \phi_i(\mathbf{x}, t) \, . \tag{1}$$

The simplest first-order statistical quantity of a two-phase random medium is its volume fraction

$$\phi_i(t) = \overline{\phi_i(\mathbf{x}, t)} \, , \tag{2}$$

where the overbar denotes ensemble averaging. Practically, we replace ensemble averages with volume averages and thus implicitly assume a statistically homogeneous system. The simplest, higher-order statistical quantity of a random, two-phase medium is given by the equal-time, two-point correlation function

$$C(\mathbf{r}, t) = \overline{\left(\phi_i(\mathbf{x} + \mathbf{r}, t) - \phi_i(t)\right)\left(\phi_i(\mathbf{x}, t) - \phi_i(t)\right)}, \tag{3}$$

which characterizes spatial fluctuations of the density around the mean. Note that $\mathbf{r}$ is a vector, so we explicitly account for anisotropic behavior. Below we restrict ourselves to the behavior along different Cartesian-coordinate directions with unit vector $\mathbf{e}_\alpha$, $\alpha = x, y, z$, and define $C_\alpha(r, t) = C(r \, \mathbf{e}_\alpha, t)$.

We note that a link to common microstructure parameters can be established via the expansion of the correlation function at the origin. In the isotropic case, for smooth interfaces the expansion

$$C(r) = \phi_i(1 - \phi_i) - \frac{s}{4} r + \frac{s}{4} \left(\frac{\overline{H^2}}{32} - \frac{\overline{K}}{96}\right) r^3 + \mathcal{O}(r^4) \tag{4}$$

is determined by the volume fraction, ϕ_i, the surface area per unit volume, s, the average squared mean curvature, $\overline{H^2}$, and the average Gaussian curvature, $\overline{K}$ (Kirste and Porod, 1962; Torquato, 2002). Higher-order terms have been omitted in the expansion, as indicated by the Landau symbol, $\mathcal{O}(r^4)$. The expansion reveals that the volume fraction and the specific surface area can only characterize spatial density fluctuations for small distances and thus provide only limited insight into the snow structure.

In order to characterize the dynamics quantitatively, we derive various length scales from the two-point correlation function. For purposes that will become clear below,

we follow Lipshtat and Meerson (2002) and employ the normalized function, $C(\mathbf{r}, t)/C(0, t)$, and define a length scale from its slope at the origin via

$$l_\alpha(t) = -\left(\frac{\mathrm{d}}{\mathrm{d}r} C_\alpha(r, t)/C_\alpha(0, t)\Big|_{r=0}\right)^{-1} . \tag{5}$$

From the expansion of the correlation function (Equation (4)) we can infer that for isotropic media in spatial dimension $d = 3$ the length scales, $l_\alpha(t)$, are related to the surface area, s per unit volume, through $\frac{\mathrm{d}}{\mathrm{d}r} C_\alpha(r, t)\Big|_{r=0} = -s/4$ for $\alpha = x, y, z$ (e.g. Torquato, 2002). Henceforth the l_α are referred to as interfacial correlation lengths. Since they determine the behavior of the correlation function at the origin, we refer to them as a characteristic on the smallest scales.

If optical properties are considered, the correlation function of snow is usually only parameterized by a single length scale (Wang and others, 1998; Mätzler, 2002), which is obtained from a fit of the correlation function to a single-scale form (e.g. an exponential). In the following we are instead guided by microstructures of disordered, bicontinuous systems. During phase ordering (Fratzl and Lebowitz, 1989) a damped oscillatory form,

$$C(r)/C(0) = \exp(-r/l) \sin\left(2\pi r/l_0\right)/(2\pi r/l_0) \, , \tag{6}$$

is predicted. The same form is also found in bicontinuous microemulsions where it is usually referred to as the Teubner–Strey form (Teubner and Strey, 1987). In addition to the interfacial correlation length, $l \sim s^{-1}$, it involves another length scale, l_0. The latter determines the first zero-crossing of the correlation function, $C(l_0) = 0$, which is usually interpreted as a typical domain size.

In view of the two-scale approximation for bicontinuous microemulsions (Equation (6)) we additionally define the first zero-crossing,

$$l_{0,\alpha}(t) = \min \left\{r | C_\alpha(r, t)/C_\alpha(0, t) = 0\right\} , \tag{7}$$

as another characteristic length scale, which is henceforth referred to as the structural correlation length. Contrary to the interfacial correlations which determine correlations on the smallest scales (at the origin), we refer to this structural correlation length as a characteristic of larger scales.

Finally, we define the ratio of ice volume and surface area as an additional length scale

$$l_{ssa}(t) = \phi_i(t)/s(t) \, . \tag{8}$$

This is simply the inverse of the specific surface area, i.e. the surface area per ice volume, which is commonly used in studies of snow metamorphism.

Thickness distribution

To compare this study with previous work, we also employ another commonly used distribution of length scales for porous media, $p_{th}(r, t)$, defined by Hildebrand and Rüegsegger (1997) as a thickness distribution. Its definition deviates from the common pore-size distribution (Torquato, 2002) and can be written as

$$p_{th}(r, t) = \overline{\delta\left(r - r_{max}(\mathbf{x})\right) \phi_i(\mathbf{x}, t)}/\phi_i(t) \, , \tag{9}$$

where $r_{max}(\mathbf{x})$ is the radius of the largest sphere that (1) contains the point $\mathbf{x}$ (not necessarily as its center) and (2) is itself contained completely in the ice phase. Note that this definition of the distribution provides an implicit
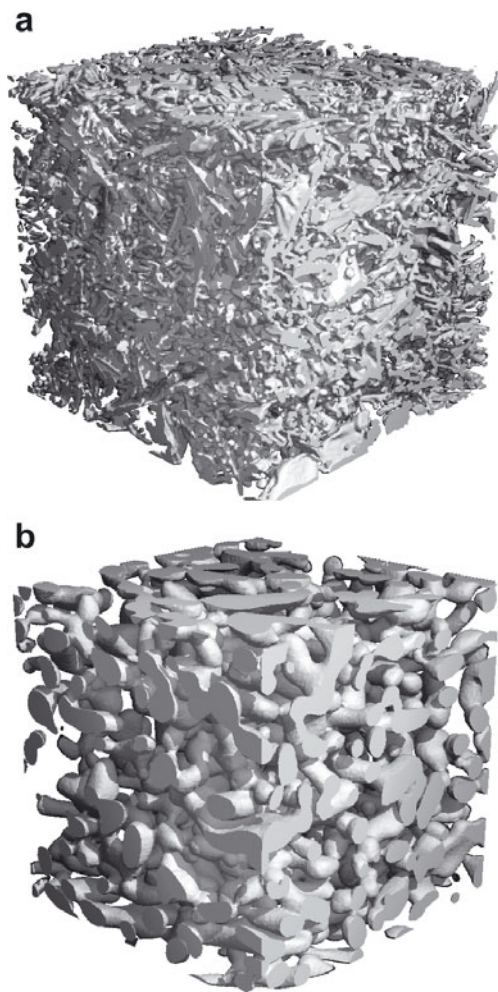
Fig. 2. Qualitative evolution of a snow cube at $T = -3°C$, (a) at the beginning and (b) at the end, after almost 1 year. The length of the cube is 5.2 mm.

definition of thickness via r_{max}. An important implication of the thickness definition is revealed by the following example. Consider a collection of non-overlapping spheres of radius r_0 which indeed implies a Dirac thickness distribution $p_{th}(r) = \delta(r - r_0)$. If the material contained in the spheres is reshaped (under volume conservation) to long cylinders of radius r_0 which are terminated by hemispherical caps at both ends, the thickness distribution remains invariant. This property will be important later when discussing the behaviour of the thickness distribution.

As a characteristic length scale of the thickness distribution we use its mean value, given by

$$l_{th}(t) = \int_0^\infty dr \, r \, p_{th}(r, t). \tag{10}$$

RESULTS

Overview

The structural analysis of the snow samples is evaluated within the $(5.2\,mm)^3$ cubic subsets (Fig. 1). With a voxel size of 10 μm this leads to lattice sizes of 520^3 voxels. A visual impression of the three-dimensional evolution of the ice matrix is shown in Figure 2. The samples evolve from bicontinuous, highly branched, fresh snow in the initial
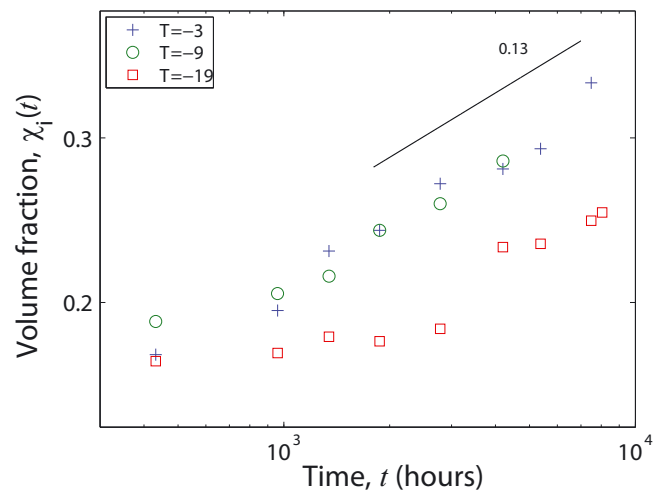
Fig. 3. Temporal evolution of the volume fraction, $\phi_i(t)$, at all temperatures.

conditions to a bicontinuous, rounded structure. Warmer samples evolve faster than colder samples.

Density

The evolution of the volume fraction (Equation (2)) of the samples is shown in Figure 3. Note the log–log scale and a guide to the eye from fitting given as a reference for a possible power-law evolution at the late stage. However, the experimental data suggest deviations from a straight line caused by modulations.
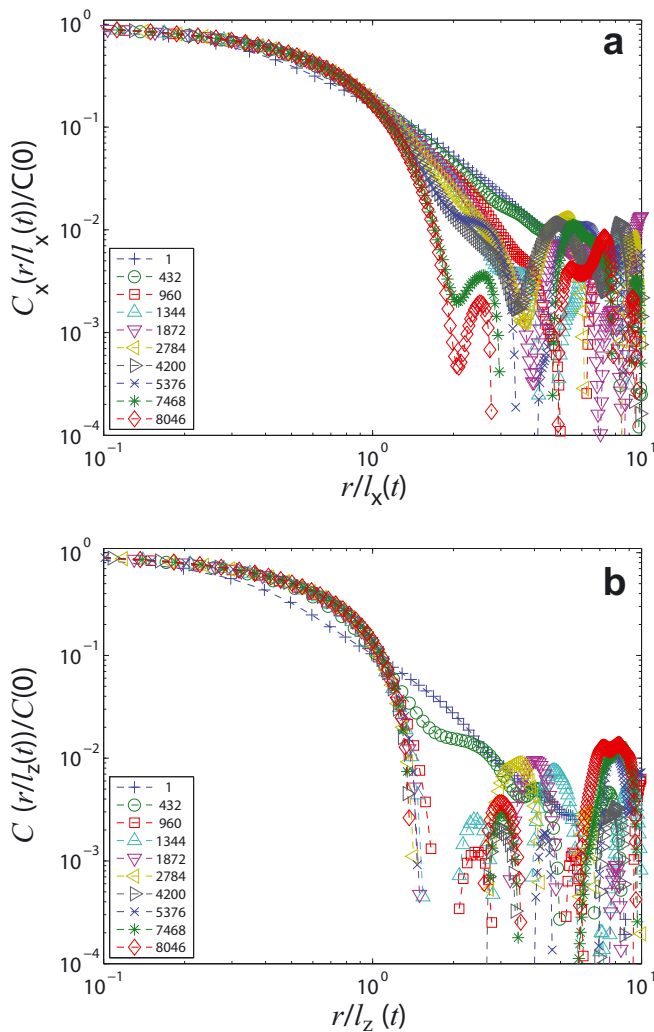
Two-point correlation function

Scaling

Here we follow Lipshtat and Meerson (2002) and normalize the correlation function (Equation (3)) by the value at the origin, $C_\alpha(r, t)/C_\alpha(0, t)$. The evolution of the two-point correlation function, $C_x(r, t)$, at $T = -3°C$ is given in Figure 4. All samples clearly display a cusp at the origin which indicates linear behavior of $C_\alpha(r, t)/C_\alpha(0, t) - 1$ on the smallest scales. This is known as the Porod law
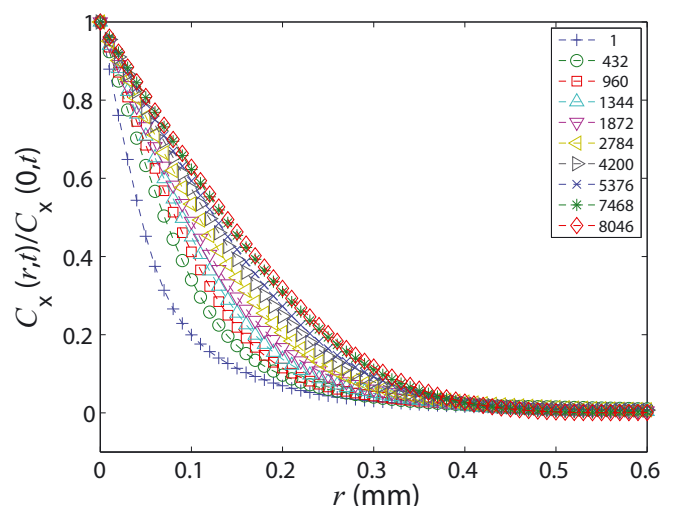
Fig. 4. Evolution of $C_x(r, t)$ at $T = -3°C$ for different times (h). On a linear scale the evolution at all temperatures appears to be similar.

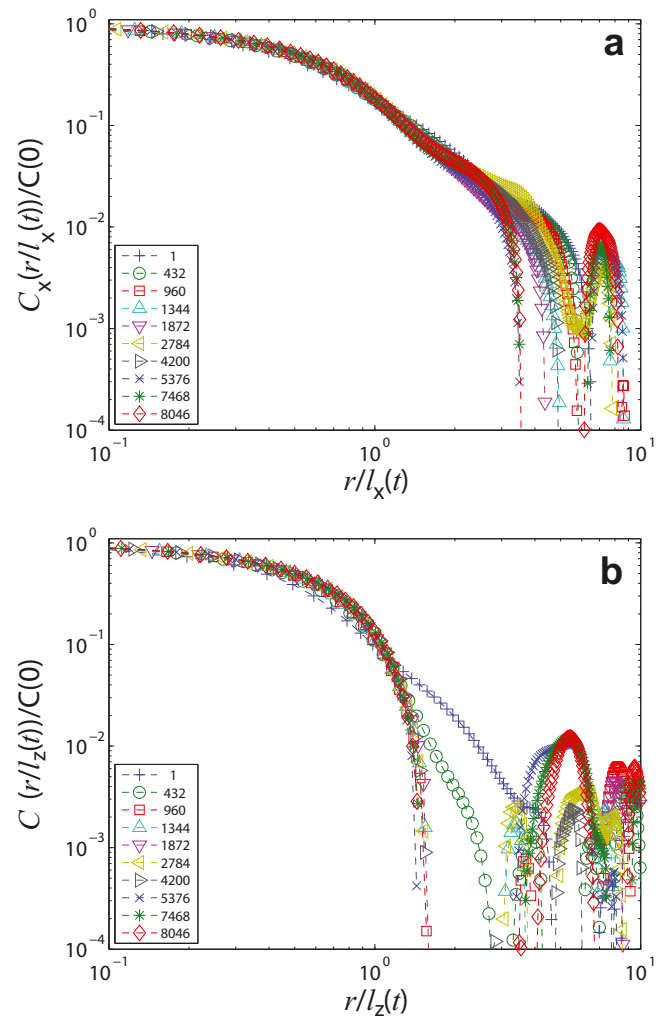**Fig. 5.** Rescaled two-point correlation functions at $T = -3°C$ for different times (h): (a) horizontal direction, C_x, and (b) vertical direction, C_z. The behavior at $T = -9°C$ is similar.

**Fig. 6.** Rescaled two-point correlation functions at $T = -19°C$ for different times (h): (a) horizontal direction, C_x, and (b) vertical direction, C_z.

(Bray, 1994), and indicates a smooth ice/vapor interface on the scale of 10 µm throughout the entire experiment. The smooth appearance of the interface on these scales has been confirmed by a comparison between X-ray tomography and gas absorption derived surface area (Kerbrat and others, 2008). We expect the accuracy of the surface area estimate at the start of the experiment to be better than the estimates for fresh snow of Kerbrat and others (2008) since our CT resolution was higher.

Next we consider the possibly anisotropic, dynamic scaling and rescale $C_\alpha(r, t)$ by the correlation lengths, $l_\alpha(t)$, which are obtained by fitting the cusp at the origin against $C_\alpha(r, t)/C_\alpha(0, t) = 1 - r/l_\alpha(t)$. These slopes increase over time, revealing a coarsening of the structure. From the perspective of dynamic scaling, the results at $T = -9°C$ cannot be distinguished from those at $T = -3°C$, so we concentrate on the comparison between $T = -3$ and $T = -19°C$. In addition, at both temperatures the x- and y-directions can be regarded as equivalent, so we concentrate on the comparison between the x- and z-directions. We explicitly note that z is the direction of gravity.

The results for the rescaled correlation functions at high temperature, $T = -3°C$, are given in Figure 5, and for the low temperature, $T = -19°C$, in Figure 6. All plots are

on a log–log scale. On a linear scale it usually remains unrevealed that the rescaled correlation functions do not fall onto a single master curve (data collapse). At the largest scales, the small number of available data points gives rise to poor statistics and an apparent stochastic behavior. However, important qualitative conclusions can be immediately drawn from the overall behavior of the correlation function at smaller scales. For both temperatures a reasonable data collapse in the z-direction is established after a short time and extends beyond the first zero-crossing, which is above $r/l_\alpha(t) \approx 1$. The zero-crossings are located in the first gap of the data in Figures 5 and 6 in the logarithmic plot. A quantitative evaluation of the zero-crossings will be presented subsequently. In contrast to the z-direction, the data collapse in the x-direction is poor and hardly extends beyond $r/l_\alpha(t) \approx 1$. The quality of scaling is only comparable with that in the z-direction at a very late stage, i.e. after almost 1 year. The overall rescaling behavior of C is poor in all cases, indicating the absence of dynamic scaling and the existence of different relevant length scales.
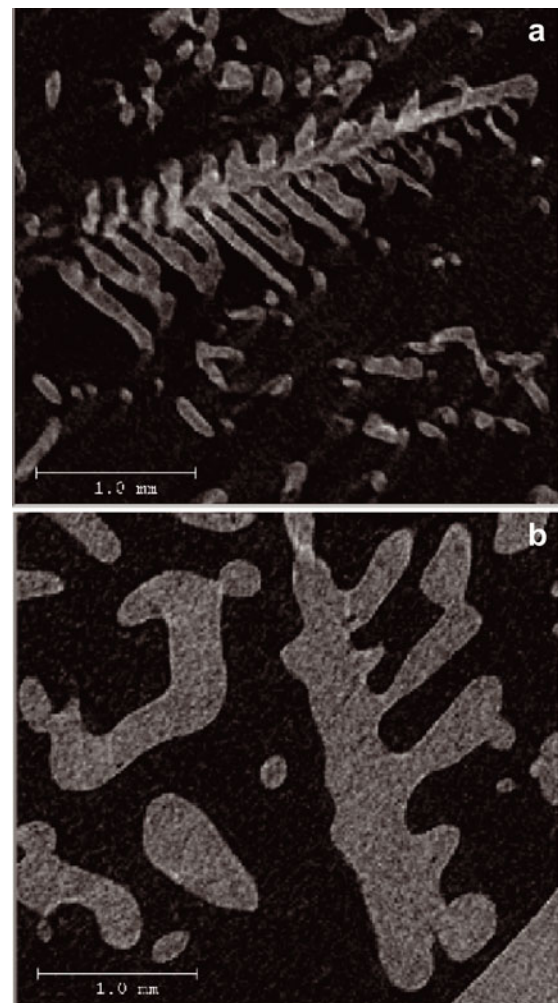
Initial condition and final state
To shed additional light on the initial condition and the final states obtained after the entire year of coarsening,
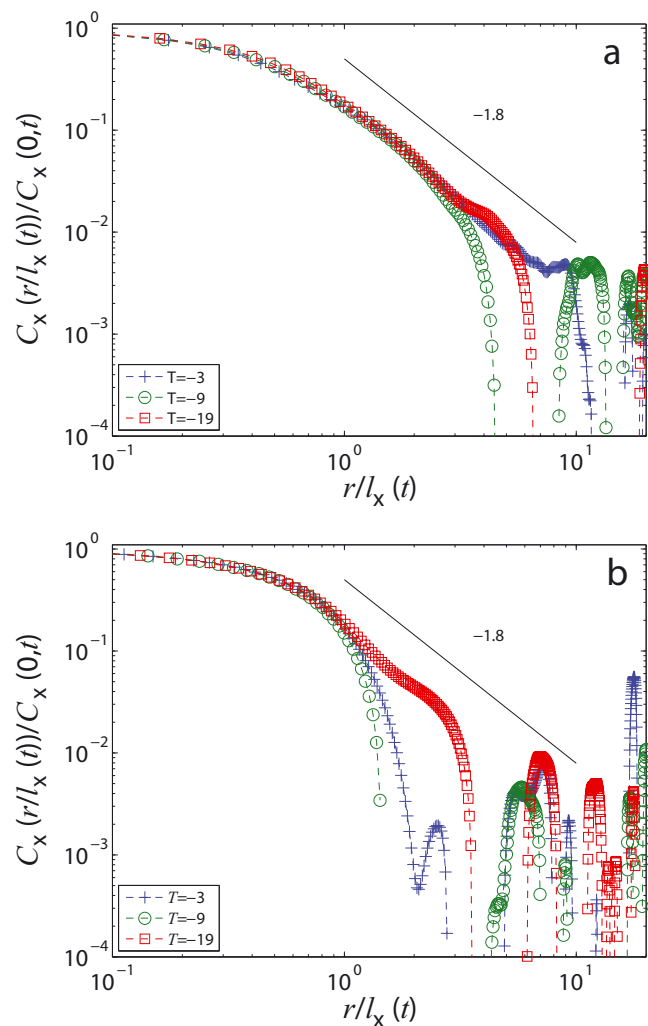
Fig. 7. Rescaled correlation functions for all temperatures (a) at the beginning and (b) at the end of the experiment.

Fig. 8. Dendritic structures in snow at $T = -19°C$ in the x-y plane. (a) Initial condition and (b) after 1 year. Note that the structures are not identical.

the correlation functions for both states are compared for all temperatures in Figure 7. Initially, correlations clearly exist beyond $r/l_\alpha(t) \approx 1$ in all three coordinate directions. The decay can be approximately described by a power law with exponent $C(r/l_\alpha(t)) \sim (r/l_\alpha(t))^{-\beta}$, with $\beta = 1.8$. This behavior is not very striking and extends only over a range of one order of magnitude. However, it clearly indicates the presence of structural correlations on scales that are large compared with $l_\alpha(t)$. The origin of these correlations is revealed by a closer, visual inspection of the sample, which shows the presence of dendritic structures, (Fig. 8). For the lowest temperature the structures persist throughout the entire year. Again by (subjective) visual inspection we confirm that after 1 year at $T = -19°C$, dendrites can only be found in the x-y plane (Fig. 8); we could not find dendritic structures from views in the x-z or y-z planes. This is in agreement with the behavior found for the correlation function (Fig. 6). In the x-direction (also in the y-direction, not shown) at $T = -19°C$ the initial power law is still visible in the form of a knee-like feature prior to the first zero-crossing of the correlation function. In contrast, in the z-direction any sign of the initial power-law correlations immediately disappears. Before investigating the time evolution of the correlation lengths in detail, we consider the distribution of ice thicknesses.
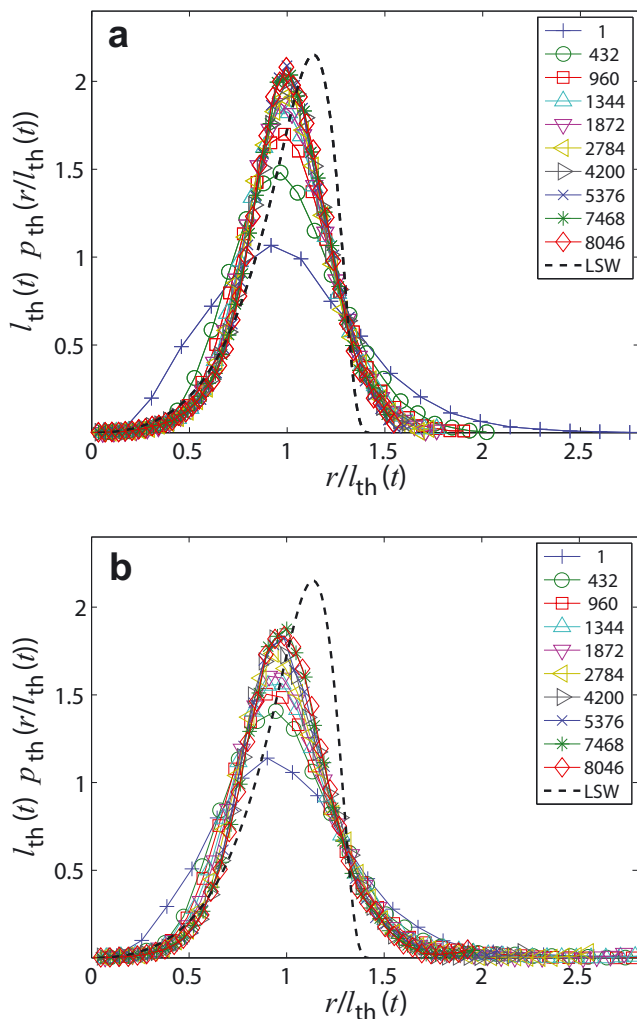
Ice-thickness distribution

Scaling

The ice-thickness distribution (Equation (9)) is computed from the vendor software of the CT device by a distance transform of the ice phase (Hildebrand and Rüegsegger, 1997). The evolution of the rescaled (by the mean l_{th}) thickness distributions is given in figure 9. Since the thickness is a measure for an approximation of the structure by spheres, we also compare the thickness distribution with the classical radius distribution of Lifshitz and Slyozov (1961), the dashed curve in Figure 9. Up to normalization the analytical form is given by $p_{LSW}(y) \sim y^2 (y + 3)^{-7/3} (3/2 - y)^{-11/3} \exp[3/(2y - 3)]$. Again we concentrate on the comparison between $T = -3$ and $-19°C$.

Initial and final state

The ice-thickness distribution of the initial and final states is shown in Figure 10, on a log-linear scale. In contrast to the correlation function, it is difficult to observe the existing correlations beyond $r/l_\alpha(t) \approx 1$ from the dendrites in the thickness distribution. This is due to the limitation that the thickness distribution does not capture the length of the cylindrical filaments (dendrite backbones), as outlined in 'Thickness distribution' in the previous section. The

Fig. 9. Rescaled ice-thickness distribution functions at (a) $T = -3°C$ and (b) $T = -19°C$ for different times (in hours).

Fig. 10. Rescaled ice-thickness distribution at (a) the beginning and (b) the end of the experiment.
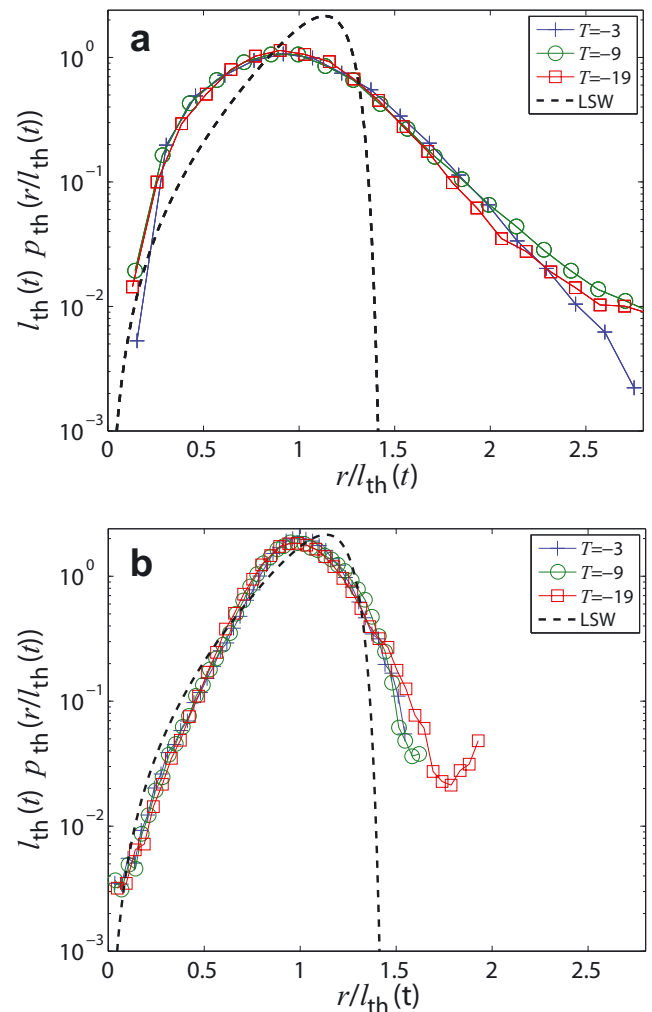
interpretation of the distribution is therefore difficult. Since $p_{th}(r, t)$ is an isotropic measure, the emerging anisotropy detected by the correlation function in different coordinate directions also remains unrevealed.

Length scales

Finally we compare the time evolution of all length scales defined in the previous section, which are derived from $C(r, t)$ and $p_{th}(r, t)$.

First we compare the interfacial correlation lengths, l_α, the mean thickness, l_{th}, and the inverse specific surface area, l_{ssa}. For a better comparison we normalize all lengths by their initial values, since absolute values of growth rates are not of interest in the present study. The various length scales are shown in Figure 11. All of them show reasonable power-law behavior with two different exponents which are given as straight black lines as a guide to the eye.

Finally, in Figure 12, we evaluate the first zeros, $l_{0,\alpha}$, of the correlation function in the x- and the z-direction, again normalized by their initial values. Interestingly, a completely different, nonmonotonic behavior is observed: the first zero of $C_z(r, t)/C_z(0, t)$ always decreases in the beginning, reaches a minimum after two time-steps and increases subsequently. The time at minimum coincides with the beginning of the onset of data collapse of the correlation

function, $C_z(r, t)/C_z(0, t)$, observed in Figures 5 and 6. In contrast, the first zeros of $C_x(r, t)/C_x(0, t)$ always display transient behavior in the beginning, which is difficult to characterize. After attaining a maximum at intermediate times, all the x curves seem to follow the slow growth of the z curves at the very late stage, where all zeros grow in unison.

DISCUSSION

General behavior of the correlation function

We start our discussion by making some general qualitative comments on the observed properties of the correlation function. In the initial state (Fig. 6a), correlations clearly extend beyond $r/l_\alpha(0) = 1$, signaling a wide distribution of length scales. The apparent power-law decay beyond $r/l_\alpha(0) = 1$ (Fig. 7) stems from the initial crystal aggregate, which contains a wide distribution of particle shapes and resembles an irregular dendritic, fractal-like morphology. During metamorphism the correlation function always evolves to an oscillating form with emerging zero-crossings. This is independent of temperature and coordinate direction. Higher-order zero-crossings are visible, but these scales are not resolved statistically with sufficient accuracy. Thus a parameterization that is characterized by a single length
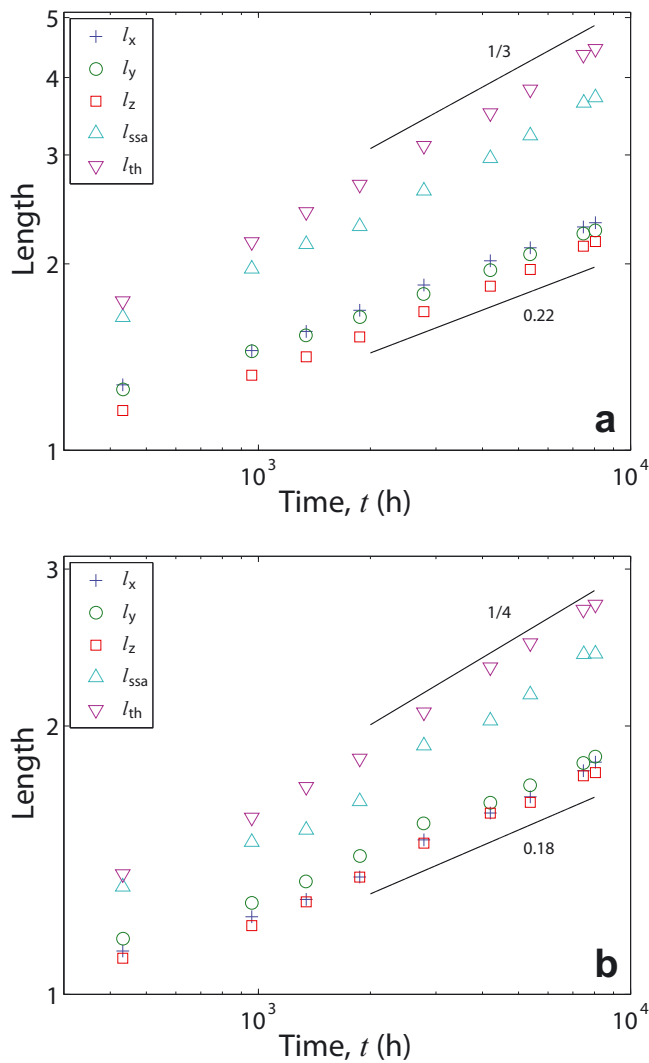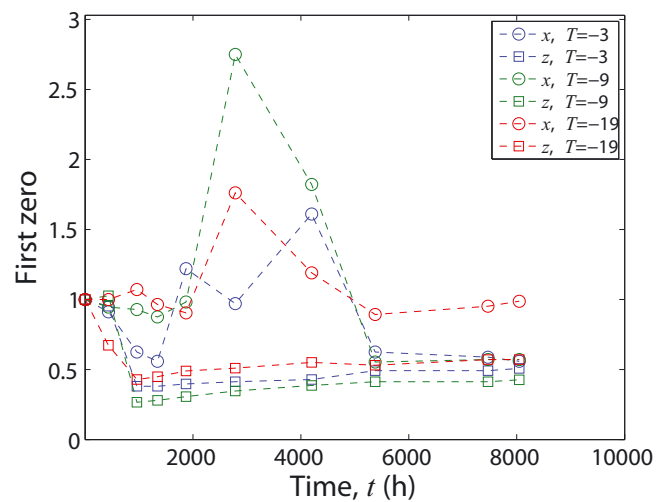
Fig. 11. Time evolution of the interfacial correlation lengths, l_α, the ice thickness, l_{th}, and the inverse specific surface area, l_{ssa}, at (a) $T = -3°C$ and (b) $T = -19°C$.

Fig. 12. Time evolution of the structural correlation lengths, $l_{0,\alpha}$, for $\alpha = x$ (circles) and $\alpha = z$ (squares), for $T = -3, -9$ and $-19°C$.

scale (Wang and others, 1998), such as the exponential form $C(r)/C(0) = \exp(-r/l)$, cannot be supported. We rather find that the slope of the correlation function at the origin and the first zero-crossing are governed by different dynamics. A detailed discussion of the distinguished dynamics of these length scales is given below. The existence of different scales requires at least a two-scale form similar to other disordered, bicontinuous systems, which can be reasonably well described by the Teubner–Strey correlation function (Equation (6)).

For a quantitative discussion we first resort to the idealized picture of phase ordering (given in the 'Theoretical background' section) and the usual assumption of dynamic scaling (Bray, 1994). This would imply a scaling form

$$C_\alpha(r, t) = f(r/l(t)) \quad (11)$$

for the correlation function at long times independent of the direction, α. Our measured correlation functions clearly reveal the breakdown of this scaling form during isothermal metamorphism of snow in all coordinate directions. This is analogous to the breakdown of scaling observed for the curvature distribution of Legagneux and Dominé (2005),

which indicates a coupling between several length scales that has to be elucidated.

Hierarchy of length scales

Our first result is the existence of different classes of length scales which can all be described by a power law, but with different exponents (Fig. 11). This is precisely the behavior reported by Lipshtat and Meerson (2002) for the coarsening of fractal clusters simulated via the Cahn–Hilliard equation. The key ingredient is the presence of power-law correlations in the initial conditions, which give rise to an additional relevant length scale during coarsening. In our case, the initial conditions contain irregular, dendritic structures. These structures are revealed in the correlation function by signatures of a power-law tail well above the interfacial correlation length, $r/l_\alpha(t) \approx 1$ (Fig. 5). The decay can roughly be described by $C(r, 0) \sim r^{-1.8}$ (Fig. 7). These correlations survive in the form of a 'knee-like' feature (a dip) in the correlation function (Figs 5 and 6) over a long period of time, as observed by Lipshtat and Meerson (2002). In the z-direction the knee-like feature almost immediately turns into a zero-crossing after two time-steps, and the correlation function shows reasonable data collapse, up to its second zero-crossing.

At high temperatures ($T = -3°C$) the observed exponent values in Figure 11a are close to $1/z = 0.33$ for l_{ssa} and l_{th}, and $1/z = 0.22$ for l_α. The smaller value for $l_\alpha(t)$ is in agreement with that obtained by Lipshtat and Meerson (2002). We note that our definition of $l_\alpha(t)$ coincides with the one given in their work, though the correlation function slightly differs: Lipshtat and Meerson (2002) consider the two-point correlation function of a single, fractal cluster with respect to the origin, which decays to zero for large distances. However, we are dealing with an assembly of these clusters, which is homogeneous on large scales. Accordingly, the two-point correlation function, as defined by Lipshtat and Meerson (2002), will decay to a nonzero value at large arguments. For comparison we have defined $C(r)$ to be the *covariance* of the random microstructure which likewise tends to zero for large arguments. The larger of our power-law exponents is close to the LSW value, $z = 3$.

At low temperatures (Fig. 11b) the scenario is qualitatively identical to the high-temperature case; only the x values of

the exponents have changed, suggesting different underlying dynamics. Here, l_{th} and l_{ssa} follow an evolution which is close to $1/z = 1/4$, whereas the exponent for the interfacial correlation lengths l_α is again well below this value. In analogy to the high-temperature case, we attribute the exponent z obtained from l_{th} and l_{ssa} to the true dynamical behavior whereas the dynamics of $l_\alpha(t)$ is subject to anomalous behavior with a larger z, due to the persistence of initial conditions. A dynamic exponent $z = 4$ is, in general, characteristic for surface diffusion (Balluffi and others, 2005), as previously suggested by Vetter and others (2010). Some support for this conjecture can be found in the work of Libbrecht (2003), where the role of surface diffusion on ice changes at $T \approx -15°C$. However, Libbrecht's work focused on the dynamics on the principal facets of ice, whereas our snow still has a round appearance, signaling the dominance of relaxations on rough orientations. On general grounds, one may expect that surface diffusion is only an intermediate dynamical regime of a surface since the $l \sim t^{1/3}$ growth due to evaporation/condensation will eventually always dominate over a $l \sim t^{1/4}$ behavior of surface diffusion. Thus it is likely that even at low temperatures a terminal LSW value of $z = 3$ is attained at even later times.

We acknowledge that the low exponents obtained for low temperatures might also be a consequence of more pronounced transients at low temperatures, as suggested by Legagneux and Dominé (2005). However, the absence of data collapse, as observed for our correlation function or for the curvature distribution of Legagneux and Dominé (2005), does not necessarily imply that the exponent is estimated incorrectly. As a counter-example, during coarsening of dendritic Pb–Sn microstructures the measured exponent attains its correct value, while curvature distributions still show transients (Kammer and Voorhees, 2006). It is reasonable that the crossover timescale, where initial conditions have died out, depends on temperature. Likewise, fitting growth laws in the same interval will lead to effective (time-dependent) dynamic exponents, $z(t) = d \ln(l)/d \ln(t)$ (Huse, 1986) and an apparently continuous increase of the measured exponents with decreasing temperature (as observed by Vetter and others, 2010). To resolve these apparently contradictory interpretations of the low values of the exponent at low temperature, experiments are required which disable the evaporation/condensation mechanism while enabling surface diffusion. This can be achieved by replacing the air in the pores by a fluid. Work along these lines is ongoing.

It is illustrative to draw the link between the observed exponent, $z = 3$, and the dynamics of a conserved order parameter. Nominating evaporation/condensation as the dominant mechanism of mass transport does not immediately imply conserved dynamics for the order parameter. It is rather the fact that the evaporation/condensation dynamics is limited by diffusion in the gas phase, which ultimately fixes $z = 3$ (Lifshitz and Slyozov, 1961). If instead the evaporation/condensation dynamics were limited by surface kinetics we would find $z = 2$ (Lifshitz and Slyozov, 1961; Wagner, 1961), though diffusion is still an indispensable component of vapor transport between successive, rate-limiting evaporation and condensation events. In the kinetics-limited regime, diffusion can be regarded as infinitely fast, hence evaporated mass is immediately available for condensation at remote parts of the structure, only subject to a global mass conservation. This effectively translates into an order parameter, which is only globally

conserved and which still leads to $z = 2$ (Lifshitz and Slyozov, 1961), similar to the dynamics in the absence of any conservation law. The kinetics-limited case requires a small condensation coefficient (Legagneux and others, 2004; Libbrecht, 2005) on the interface and thus the result $z = 3$ is consistent with diffusion-limited evaporation/condensation.

Despite the absence of dynamic scaling, all length scales discussed so far display a monotonic increase. They can be reasonably well described by a power law which is the same for all coordinate directions. A completely different behavior is observed for the structural correlation lengths, $l_{0,\alpha}$, which are nonmonotonic and anisotropic. Remarkably, the observed anisotropy between the rescaling properties of $C(r, t)$ in the z- and the x-direction (Figs 5 and 6) has no influence on the evolution of the interfacial correlation lengths, l_α, in the respective directions (Fig. 11). This implies that the dynamics on the smallest scales remains isotropic. In general, one can expect a dependence of the growth rate of l_α on the volume fraction (Ratke and Voorhees, 2002) and thus implicitly a dependence on time. However, this effect cannot be resolved from our data. The isotropy on the smallest scales holds true at all temperatures and suggests that the anisotropy emerges from larger scales. This is confirmed by the evolution of the first zero-crossing, $l_{0,\alpha}$, of $C_\alpha(r, t)/C(0, t)$, which displays a complicated, anisotropic behavior. Since gravity is the only mechanism that breaks the symmetry between horizontal and vertical directions it is likely to be the origin of the anisotropy. Usually, the zero-crossing is interpreted as a typical domain size (Teubner and Strey, 1987). Hence one can define $\Omega(t) = (l_{0,x}, l_{0,y}, l_{0,z})$ as an oriented structural unit of the ice network. The dynamics of $\Omega(t)$ characterizes the evolution of some orientational order which does not show any qualitative differences between different temperatures (Fig. 12). The z-component of $\Omega(t)$ always decreases rapidly, followed by a slow monotonic increase. The rapid decrease might be caused by some rotational motion under gravity. This might be corroborated by the fact that after 1 year the long arm of the dendrite is predominantly found in the x-y plane. In contrast, the x, y components of Ω initially show some transient behavior which is followed by a maximum where correlations roughly double when compared to the initial value. The temporal resolution is too coarse to investigate this phenomenon in quantitative detail, but the qualitative features of the evolution are present at all temperatures. A quantitative investigation of these structural rearrangements, their possible impact on modulations of the bulk densification rate and their possible initiation by interfacial-scale coarsening is left for future work.

Relation to curvature distributions of snow

The observed properties of the correlation function can be discussed in connection with interfacial curvature distributions which are sometimes used to characterize the evolution of snow (Flin and others, 2003; Legagneux and others, 2004). Similar to our case, those authors observe the absence of scaling of the curvature distribution. It is likely that their distributions are also influenced by larger-scale structural rearrangements or the persistence of initial conditions. Our analysis above suggests that this is an implication of the structural reorganization at larger scales and thus cannot be predicted by coarsening mechanisms alone. Previous work on isothermal metamorphism has usually focused on the specific surface area and its

interpretation in terms of modified LSW approaches. The expansion of Equation (4) unambiguously reveals that the specific surface area only describes spatial correlations of snow on the smallest scales. This appears to be insufficient, due to the existence of different relevant length scales which are influenced by memory effects of initial conditions or gravity. A first attempt to include gravity in isothermal metamorphism has been made using Monte Carlo simulations (Vetter and others, 2010). Future effort in this direction is highly desirable. Apparently, the structural ordering on larger scales leaves the interfacial phase ordering nearly unaffected. This can be inferred from Figures 10 and 11. While the interfacial scales already evolve monotonically (beyond $t = 2000$ hours), the structural scales still display nonmonotonic and anisotropic behavior. This suggests an appealing simplification for modeling macroscopic densification: one might solely focus on how structural mobility is induced by small-scale interfacial coarsening, which can be regarded as externally imposed.

Relation to radiative properties of snow

Finally, we comment on a possible application of our results to field measurements. The Fourier transform of the correlation function naturally emerges in certain approximations for the scattered intensity of radiation in snow as a random medium (Vallese and Kong, 1981; Mätzler, 1998; Arslan and others, 2005). Thereby ad hoc assumptions for the functional form of the correlation function are employed to match the measured intensity with a single length scale and microstructural information is commonly required to provide this length scale. If these steps were to be reversed, more accurate microstructural information could be obtained from optical measurements in the field. However, a procedure analogous to small-angle scattering (Debye and Bueche, 1949) will be difficult, since relevant structural length scales of snow fall precisely into the wavelengths of the far-infrared spectrum in which ice strongly absorbs.

CONCLUSIONS

We have employed the density correlatio function to investigate the dynamics of direction-dependent spatial fluctuations of the microscopic density of snow during isothermal metamorphism. The observed correlation function always evolves to a state where the decay of correlations is modulated by oscillations indicating a certain order, i.e. alternating arrangement of ice and pores. Thus non-negative, single-scale parameterizations, such as an exponential form for the correlation function, seem to be inaccurate. Different types of dynamics have been revealed by closer inspection of the slope and the first zero-crossing of the correlation function. The behavior of the slope of the correlation function is quantitatively reminiscent of coarsening of fractal clusters and argued to be a consequence of dendritic initial conditions which persist at low temperatures over an entire year. The similarities between dendritic and fractal coarsening must, however, be further elucidated. The dynamics of the specific surface area seem to be governed by the 'true' dynamic exponent which suggests the dominant underlying pathway of mass transport: diffusion-limited evaporation/condensation with $z = 3$ at high temperatures, and surface diffusion with $z = 4$ at low temperatures. The slowing down of growth might be likewise caused by continuously increasing transients to a final scaling state.

With regard to applications it will be interesting to see whether the two-scale Teubner–Strey form of the correlation function provides missing geometrical information for scattering problems.

REFERENCES

Arnaud, L., J.M. Barnola and P. Duval. 2000. Physical modeling of the densification of snow/firn and ice in the upper part of polar ice sheets. *In* Hondoh, T., *ed. Physics of ice core records.* Sapporo, Hokkaido University Press, 285–305.

Arslan, A.N., M.T. Hallikainen and J.T. Pullinainen. 2005. Investigating of snow wetness parameter using a two-phase backscattering model. *IEEE Trans. Geosci. Remote Sens.*, **43**(8), 1827–1833.

Balluffi, R.W., S.M. Allen and W.C. Carter. 2005. *Kinetics of materials.* Hoboken, NJ, Wiley.

Blackford, J.R. 2007. Sintering and microstructure of ice: a review. *J. Phys. D*, **40**(21), R355–R385.

Bray, A.J. 1994. Theory of phase-ordering kinetics. *Adv. Phys.*, **43**(3), 357–459.

Debye, P. and A.M. Bueche. 1949. Scattering by an inhomogeneous solid. *J. Appl. Phys.*, **20**(6), 518–525.

Dominé, F. *and 6 others.* 2003. Snow metamorphism as revealed by scanning electron microscopy. *Microsc. Res. Tech.*, **62**(1), 33–48.

Flin, F., J.B. Brzoska, B. Lesaffre, C. Coléou and R.A. Pieritz. 2003. Full three-dimensional modelling of curvature-dependent snow metamorphism: first results and comparison with experimental tomographic data. *J. Phys. D*, **36**(10A), A49–A54.

Flin, F., J.-B. Brzoska, B. Lesaffre, C. Coléou and R.A. Pieritz. 2004. Three-dimensional geometric measurements of snow microstructural evolution under isothermal conditions. *Ann. Glaciol.*, **38**, 39–44.

Fratzl, P. and J.L. Lebowitz. 1989. Universality of scaled structure functions in quenched systems undergoing phase separation. *Acta Metall.*, **37**(12), 3245–3248.

Furukawa, Y. and J.S. Wettlaufer. 2007. Snow and ice crystals. *Phys. Today*, **60**(12), 70–71.

Gow, A.J. 1969. On the rates of growth of grains and crystals in South Polar firn. *J. Glaciol.*, **8**(53), 241–252.

Hildebrand, T. and P. Rüegsegger. 1997. A new method for the model-independent assessment of thickness in three-dimensional images. *J. Microsc.*, **185**(1), 67–75.

Huse, D.A. 1986. Corrections to late-stage behavior in spinodal decomposition: Lifshitz–Slyozov scaling and Monte Carlo simulations. *Phys. Rev. B*, **34**(11), 7845–7850.

Kaempfer, T.U. and M. Plapp. 2009. Phase-field modeling of dry snow metamorphism. *Phys. Rev. E*, **79**(3), 031502. (10.1103/PhysRevE.79.031502.)

Kaempfer, T.U. and M. Schneebeli. 2007. Observation of isothermal metamorphism of new snow and interpretation as a sintering process. *J. Geophys. Res.*, **112**(D24), D24101. (10.1029/2007JD009047.)

Kaempfer, T.U., M. Schneebeli and S.A. Sokratov. 2005. A microstructural approach to model heat transfer in snow. *Geophys. Res. Lett.*, **32**(21), L21503. (10.1029/2005GL023873.)

Kammer, D. and P.W. Voorhees. 2006. The morphological evolution of dendritic microstructures during coarsening. *Acta Mater.*, **54**(6), 1549–1558.

Kerbrat, M., B. Pinzer, T. Huthwelker, H.W. Gäggeler, M. Ammann and M. Schneebeli. 2008. Measuring the specific surface area of snow with X-ray tomography and gas adsorption: comparison

and implications for surface smoothness. *Atmos. Chem. Phys.*, **8**(5), 1261–1275.

Kirste, R. and G. Porod. 1962. Röntgenkleinwinkelstreuung an kolloiden Systemen: asymptotisches Verhalten der Streukurven. *Kolloid-Z. Z. Polym.*, **184**(1), 1–7.

Kwon, Y., K. Thornton and P.W. Voorhees. 2007. Coarsening of bicontinuous structures via nonconserved and conserved dynamics. *Phys. Rev. E*, **75**(2), 021120. (10.1103/PhysRevE.75.021120.)

Legagneux, L. and F. Dominé. 2005. A mean field model of the decrease of the specific surface area of dry snow during isothermal metamorphism. *J. Geophys. Res.*, **110**(F4), F04011. (10.1029/2004JF000181.)

Legagneux, L., A.-S. Taillandier and F. Dominé. 2004. Grain growth theories and the isothermal evolution of the specific surface area of snow. *J. Appl. Phys.*, **95**(11, Pt 1), 6175–6184.

Libbrecht, K.G. 2003. Growth rates of the principal facets of ice between $-10°C$ and $-40°C$. *J. Cryst. Growth*, **247**(3–4), 530–540.

Libbrecht, K.G. 2005. The physics of snow crystals. *Rep. Progr. Phys.*, **68**(4),855–895.

Lifshitz, I.M. and V.V. Slyozov. 1961. The kinetics of precipitation from supersaturated solid solutions. *J. Phys. Chem. Solids*, **19**(1–2), 35–50.

Lipshtat, A. and B. Meerson. 2002. Anomalous dynamic scaling in locally conserved coarsening of fractal clusters. *Phys. Rev. E*, **65**(5), 050501. (10.1103/PhysRevE.65.050501.)

Löwe, H., L. Egli, S. Bartlett, M. Guala and C. Manes. 2007. On the evolution of the snow surface during snowfall. *Geophys. Res. Lett.*, **34**(21), L21507. (10.1029/2007GL031637.)

Mätzler, C. 1998. Improved Born approximation for scattering in a granular medium. *J. Appl. Phys.*, **83**(11), 6111–6117.

Mätzler, C. 2002. Relation between grain-size and correlation length of snow. *J. Glaciol.*, **48**(162), 461–466.

Mendoza, R., J. Alkemper and P.W. Voorhees. 2005. Three-dimensional morphological characterization of coarsened microstructures. *Z. Metallkd*, **96**(2), 155–160.

Nakamura, H. 1978. New apparatus to produce fresh snow. *Rep. Nat. Res. Cent. Disaster Prev.* 19. 229–237. [In Japanese with English summary.]

Ratke, L. and P.W. Voorhees. 2002. *Growth and coarsening: ripening in material processing.* Berlin, etc., Springer-Verlag.

Saito, Y. 1996. *Statistical physics of crystal growth.* Singapore, World Scientific.

Teubner, M. and R. Strey. 1987. Origin of the scattering peak in microemulsions. *J. Chem. Phys.*, **87**(5), 3195–3200.

Torquato, S. 2002. *Random heterogeneous materials: microstructure and macroscopic properties.* New York, Springer-Verlag.

Vallese, F. and J.A. Kong. 1981. Correlation-function studies for snow and ice. *J. Appl. Phys.*, **52**(8), 4921–4925.

Vetter, R., S. Sigg, H.M. Singer, D. Kadau, H.J. Herrmann and M. Schneebeli. 2010. Simulating isothermal aging of snow. *Europhys. Lett.*, **89**(2), 26001. (10.1209/0295-5075/89/26001.)

Wagner, C. 1961. Theorie der Alterung von Niederschlägen durch Umlösen (Ostwald-Reifung). *Z. Elektrochem.*, **65**(7–8), 581–591.

Wang, H., J. Pulliainen and M. Hallikainen. 1998. Correlation functions and correlation lengths for dry snow. *J. Electromag. Waves Appl.*, **12**(10), 1337–1347.

Wang, K.G. 2008. Unified model equations for microstructure evolution. *Physica A*, **387**(13), 3084–3092.

Westbrook, C.D., R.C. Ball, P.R. Field and A.J. Heymsfield. 2004. Theory of growth by differential sedimentation, with application to snowflake formation. *Phys. Rev. E*, **70**(2), 021403. (10.1103/PhysRevE.70.021403.)

Yuan, H., J.H. Lee and J.E. Guilkey. 2010. Stochastic reconstruction of the microstructure of equilibrium form snow and computation of effective elastic properties. *J. Glaciol.*, **56**(197), 405–414.